We are IntechOpen,
the world's leading publisher of
Open Access books
Built by scientists, for scientists

6,000
Open access books available

148,000
International authors and editors

185M
Downloads

154
Countries delivered to

Our authors are among the

TOP 1%
most cited scientists

12.2%
Contributors from top 500 universities

CLARIVATE ANALYTICS
BOOK CITATION INDEX
INDEXED

WEB OF SCIENCE™

Selection of our books indexed in the Book Citation Index
in Web of Science™ Core Collection (BKCI)

Interested in publishing with us?
Contact book.department@intechopen.com

Chapter

Amplitude-Dependent Acoustic Absorber

Jiangyi Zhang

Abstract

In this chapter, we consider the design of 1D amplitude-dependent acoustic absorber, i.e., acoustic metamaterial composed of an air-filled waveguide periodically side-loaded by holes. Firstly we present experimental results about high-amplitude sound wave propagation in the structure. We find that there is not only the linear viscothermal and radiation losses, but also the nonlinear losses. High-amplitude sound waves at the locations of the side holes could introduce nonlinear losses, which is due to the geometrical discontinuity. This phenomenon could be found in experiments about amplitude-dependent reflection, transmission, and absorption coefficients. The experimental results show the possibility to use the system as a nonlinear absorber, that is, nonlinear losses change the nature of the device from a reflective to an absorbing one. Our results reveal the role of nonlinear losses in the proposed device and also provide a quite accurate analytical model to capture the effect of such losses. In the end, we analytically tune the parameters of the device and design 1D amplitude-dependent acoustic absorber.

Keywords: nonlinear losses, nonlinear acoustic absorber, acoustic metamaterial, transfer matrix method, acoustic waveguide

1. Introduction

In the nature, the properties of conventional materials depend on the composing atoms/molecules and the chemical bonds, while their physical properties such as mass density and bulk modulus are always positive. Metamaterials, namely periodic or random man-made structures composed of meta-atoms, for example, sub-wavelength resonators the size of which is bigger than the atomic scale but much smaller than the relevant radiated wavelength, are designed to exhibit exotic properties not commonly found in nature. The physical properties of metamaterials are described by effective parameters which could be positive, negative, near-zero or approaching-infinity [1]. The concept of metamaterials was firstly theorized by the Russian physicist Veselago [2] for electromagnetic waves in 1968. He considered the possible existence of metamaterials with simultaneously negative permittivity and permeability, i.e., left-handed materials or double negative metamaterials. In 2000, Liu et al. firstly introduced the concept of acoustic metamaterials [3]. Later, acoustic metamaterials have been widely developed to deeply control and manipulate waves due to their exotic

properties not found in nature. As a result, a plethora of applications has been developed, including acoustic diodes [4, 5], acoustic lenses for sub-diffraction imaging [6], acoustic sound focusing based on gradient index lenses [7–9], acoustic topological systems [10–12] and acoustic cloaking [13–15].

Wave propagation in acoustic metamaterials is subject to losses such as visothermal losses at the solid-fluid interface [16], which can have deleterious consequences. For example, Heríquez et al. [17] found that viscothermal losses could destroy the predicted behavior of double negative acoustic metamaterials designed by Gracía-Salgado et al. [18], and they even speculated that rigid-based metamaterials could become absorbers in particular situations. Previously, Guild et al. [19] and Romero-Garcá et al. [20] proposed specific acoustic metamaterials absorbers based on dissipative effect. Losses could also change the dispersion relation of the system. For example, Theocharis et al. [21] show that near-zero group velocity dispersion band disappears in the presence of the viscothermal losses. Thus, losses are non-negligible in such kind of materials and should be not ignored. Perfect and broadband absorber is an important branch of acoustic metamaterials [20, 22].

In the field of metamaterials, only few studies exist regarding nonlinear effects. In 2003, Lapine et al. proposed the concept of nonlinear metamaterials in the field of electromagnetism [23]. During the last years, the study of nonlinear acoustic metamaterials received increased attention [24–26]. In the case of acoustic metamaterials, the presence of nonlinearity is easily introduced at high acoustic levels. Accompanying with wave propagation, the localized pressure changes. High pressure increases the local temperature, and the local speed of sound in the compressible material is proportional to the temperature [27]. As a result, the wave with high pressure phase travels faster compared to a wave of low pressure phase. During the nonlinear wave propagation, higher harmonics are generated. Dispersion effect introduced by the resonators and periodicity of the acoustic metamaterials could tailor the source and generated harmonics. Thus, one can observe the beating of higher generated harmonics [28–30]. Acoustic diodes have been also designed based on the combination of nonlinearity and dispersion. Liang et al. realized the nonreciprocal acoustic transmission by breaking the linearity, which violates some assumptions of Onsager-Casimir principle [4]. In granular crystals, Boechler et al. envisaged the bifurcation-based acoustic switching and rectification [31]. Devaux et al. achieved asymmetric acoustic propagation by a nonlinear self-demodulation effect [32]. There are many other nonlinear processes, for example, the nonlinear dispersion relation [33], nonlinear acoustic lenses [34], waves coupling in nonlinear metamaterials [35], discrete breathers [36], the self-demodulation effect [37, 38], and the formation of acoustic solitons of various types-pulse-like [39, 40] and envelope ones [40, 41], namely robust localized waves propagating undistorted due to a balance between dispersion and nonlinearity.

Despite this extensive body of nonlinear acoustic metamaterials and acoustic absorbers, only few works consider nonlinear losses. However, in acoustics, nonlinear losses may easily appear, e.g., due to the geometrical discontinuity [42, 43]. In this article, we design 1D amplitude-dependent acoustic absorber made by an air-filled waveguide periodically side-loaded by holes with sharp edges. These sharp edges can be considered as geometrical discontinuities, which could introduce nonlinear losses. Based on the accurate analytical model which could predict the experimental results, we tune the parameters of the device in order to design a nonlinear perfect absorber. Particularly the industry is concerned about the perfect absorber in low frequencies. However, nonlinear losses could change the nature of the device from reflective one to an absorber, especially in low frequencies.

This chapter is structured as follows. In Section 2, we introduce the setup and the method of processing the experimental data. In Section 3, we derive the analytical model based on transfer matrix method. In Section 4, we discuss the experimental phenomenon and analytical model. Based on results obtained, we tune the parameters of the device in order to design an 1D amplitude-dependent acoustic perfect absorber in low frequencies. Finally Section 5 summarizes the findings and discusses future research directions.

2. Experiments

2.1 Experimental set-up

Figure 1 shows the experimental set-up in order to characterize the amplitude-dependent reflection, transmission and absorption coefficient. This system is an air-filled acoustic cylindrical waveguide periodically loaded by side-holes. The length of the waveguide is 3 m; the internal radius is $r = 0.025$ m; there is 40 side-holes; the distance between two side holes is $d = 0.05$ m; the radius of the side holes is $r_H = 0.0035$ m and the length is $l_H = 0.005$ m. We use white noise with frequencies from 200 Hz to 1000 Hz as source. In order to avoid back reflections in the waveguide, we use a properly designed anechoic termination [21, 45], and do the experiments in an anechoic room.

We perform four experiments with different source amplitudes. Here we use a four microphone method [46] to obtain the transmission, reflection and absorption coefficient. We put two microphones (1/2 inch *B&K*) at the one end of the wave-guide; and another two microphones on other side of the structure, shown in **Figure 1**. This method allows the measurement of both the forward and backward waves for the fundamental frequency.
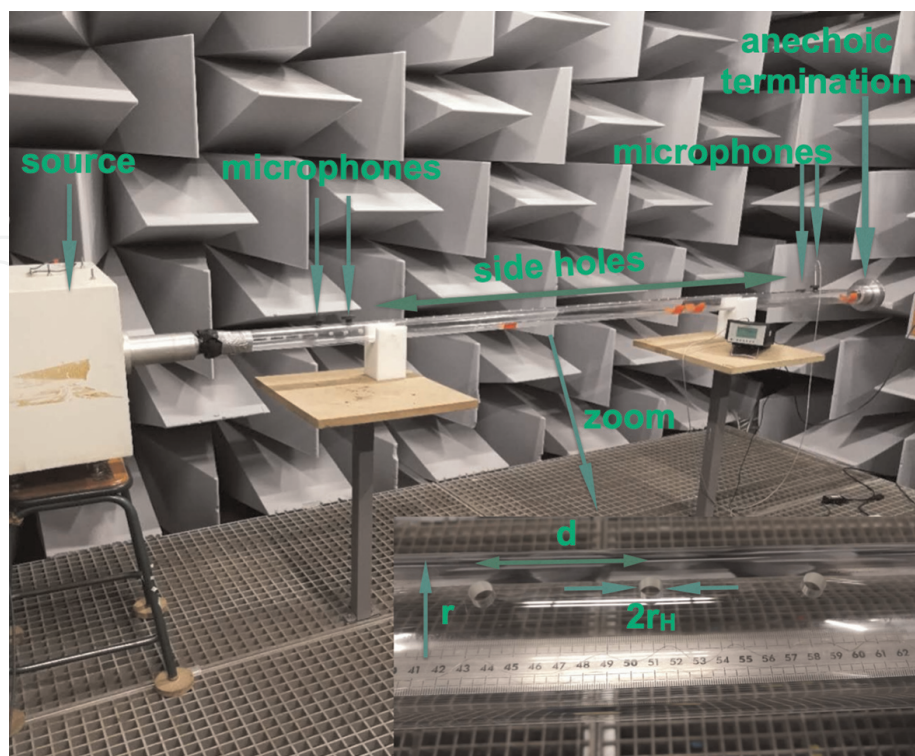

Figure 1.
(color online) picture of the experimental setting for the measurement of the amplitude-dependent reflection, transmission and absorption coefficients, adapted from ref. [44].

2.2 Experimental data processing

Here are the details of four microphone method. p_1, p_2, p_3 and p_4 present the complex sound pressure measured by the microphones at x_1, x_2, x_3 and x_4 in **Figure 2**, with $x_1 = 0.2$ m, $x_2 = 0.1$ m, $x_3 = 2.1$ m and $x_4 = 2.2$ m respectively. Acoustic pressures measured by the microphone comprise various superpositions of positive- and negative-going plane waves in the waveguide,

$$
\begin{aligned}
p_1 &= \left(Ae^{-jkx_1} + Be^{jkx_1}\right)e^{i\omega t}, \\
p_2 &= \left(Ae^{-jkx_2} + Be^{jkx_2}\right)e^{i\omega t}, \\
p_3 &= \left(Ce^{-jkx_3} + De^{jkx_3}\right)e^{i\omega t}, \\
p_4 &= \left(Ce^{-jkx_4} + De^{jkx_4}\right)e^{i\omega t},
\end{aligned}
\tag{1}
$$

where A and B (C and D) are the amplitudes of the positive- and negative going plane wave at the beginning (ending) of the waveguide respectively, which could be derived from Eq.(1),

$$
\begin{aligned}
A &= \frac{j\left(p_1 e^{jkx_2} - p_2 e^{jkx_1}\right)}{2\sin k(x_1 - x_2)}, \\
B &= \frac{j\left(p_2 e^{-jkx_1} - p_1 e^{-jkx_2}\right)}{2\sin k(x_1 - x_2)}, \\
C &= \frac{j\left(p_3 e^{jkx_4} - p_4 e^{jkx_3}\right)}{2\sin k(x_3 - x_4)}, \\
D &= \frac{j\left(p_4 e^{-jkx_3} - p_3 e^{-jkx_4}\right)}{2\sin k(x_3 - x_4)},
\end{aligned}
\tag{2}
$$

and provide the input data for subsequent transfer matrix calculations.
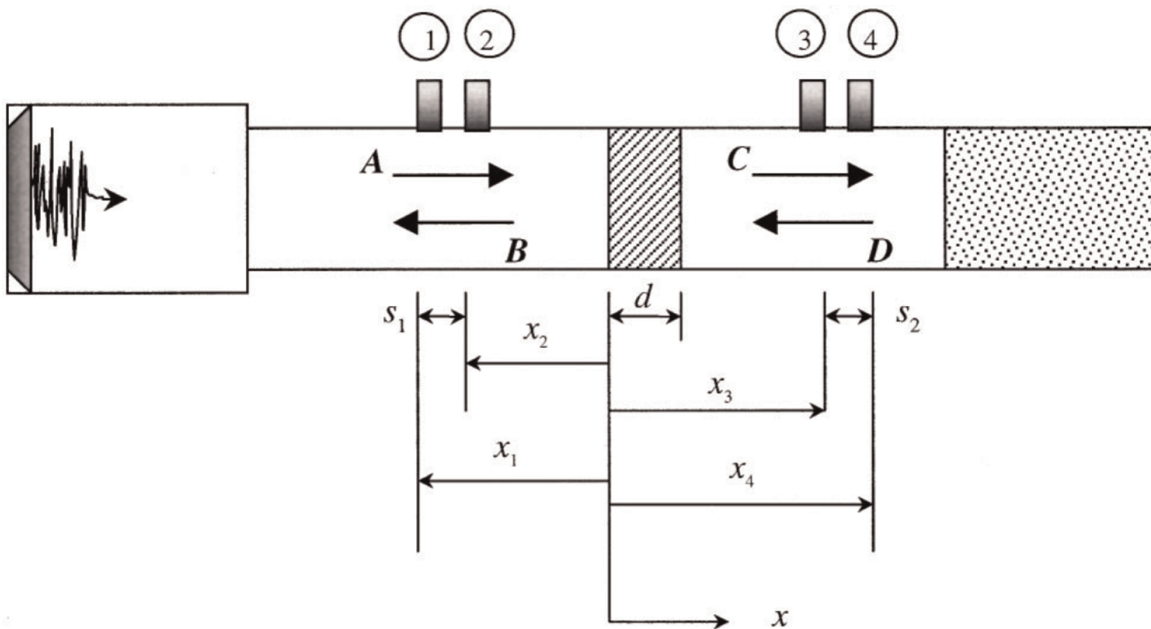

Figure 2.
Schematic diagram of the standing wave tube, adapted from ref. [46].

To relate the sound pressures and velocities on the two faces of 40 side holes, transfer matrix is used, extending from $x = 0$ to $x = 40^*d$, as shown in **Figure 2**, i.e.,

$$\begin{bmatrix} p \\ v \end{bmatrix}_{x=0} = \begin{bmatrix} T_{11} & T_{12} \\ T_{21} & T_{22} \end{bmatrix} \begin{bmatrix} p \\ v \end{bmatrix}_{x=40d}, \tag{3}$$

where $p|_{x=0}$, $v|_{x=0}$, $p|_{x=40d}$ and $v|_{x=40d}$ may easily be expressed in terms of the positive- and negative-going plane wave component amplitude, i.e.,

$$p\Big|_{x=0} = A + B, v\Big|_{x=0} = \frac{A - B}{\rho_0 c} p\Big|_{x=40d} = Ce^{-jk40d} + De^{jk40d}, v\Big|_{x=40d} = \frac{Ce^{-jk40d} - De^{jk40d}}{\rho_0 c}.$$

$$\tag{4}$$

Eq. (3) presents two equations with four unknowns, T_{11}, T_{12}, T_{21} and T_{22}. In order to solve the transfer matrix elements, we need two additional equations, which could be generated by reciprocity and symmetry nature of the material. Pierce noted that reciprocity requires that the determinant of the transfer matrix be unity [46, 47],

$$T_{11}T_{22} - T_{12}T_{21} = 1,$$

and for symmetrical system,

$$T_{11} = T_{22}.$$

Then the transfer matrix elements are solved,

$$T_{11} = \frac{p|_{x=40d}v|_{x=40d} + p|_{x=0}v|_{x=0}}{p|_{x=0}v|_{x=40d} + p|_{x=40d}v|_{x=0}},$$

$$T_{12} = \frac{p|^2_{x=0} - p|^2_{x=40d}}{p|_{x=0}v|_{x=40d} + p|_{x=40d}v|_{x=0}},$$

$$T_{21} = \frac{v|^2_{x=0} - v|^2_{x=40d}}{p|_{x=0}v|_{x=40d} + p|_{x=40d}v|_{x=0}}, \tag{5}$$

$$T_{22} = \frac{p|_{x=40d}v|_{x=40d} + p|_{x=0}v|_{x=0}}{p|_{x=0}v|_{x=40d} + p|_{x=40d}v|_{x=0}},$$

which provide the input data for subsequent reflection and transmission coefficients calculations.

In order to calculate reflection and transmission coefficients, we assume that the incidental plane wave has unit amplitude, and the termination is anechoic, so that we could consider the parameter D is negligible compared to parameter C. Thus we could write,

$$p\Big|_{x=0} = 1 + R, v\Big|_{x=0} = \frac{1 - R}{\rho_0 c} p\Big|_{x=40d} = Te^{-jk40d}, v\Big|_{x=40d} = \frac{Te^{-jk40d}}{\rho_0 c}, \tag{6}$$

where $R = B/A$ and $T = C/A$ are the reflection and transmission coefficients respectively. When we substituted Eq.(6) into Eq.(3), the transmission T and reflection coefficient R for the case of an anechoic termination, can be respectively expressed as,

$$T = \frac{2e^{jkd}}{T_{11} + (T_{12}/\rho_0 c) + \rho_0 c T_{21} + T_{22}}, \tag{7}$$

$$R = \frac{T_{11} + (T_{12}/\rho_0 c) - \rho_0 c T_{21} - T_{22}}{T_{11} + (T_{12}/\rho_0 c) + \rho_0 c T_{21} + T_{22}}, \tag{8}$$

and the absorption coefficient is

$$\alpha = 1 - T^2 - R^2. \tag{9}$$

Through the above data processing, we obtain the experimental amplitude-dependent reflection, transmission and absorption coefficients. The corresponding results are shown in Section 4.

3. Transfer matrix method

In this section, we analytically use transfer matrix method to capture the amplitude-dependent reflection, transmission and absorption coefficients. The transfer matrix T used to relate the sound pressures and velocities on the two faces of the acoustic waveguide with the N side holes, can be written as

$$T = \prod_{n=1}^{N} T_n \tag{10}$$

where

$$
T_n =
\begin{bmatrix}
\cos\left(\dfrac{k_{ph}d}{2}\right) & iZ_c \sin\left(\dfrac{k_{ph}d}{2}\right) \\
\dfrac{i}{Z_c} \sin\left(\dfrac{k_{ph}d}{2}\right) & \cos\left(\dfrac{k_{ph}d}{2}\right)
\end{bmatrix}
\begin{bmatrix}
1 & 0 \\
\dfrac{1}{Z_{H(n)}} & 1
\end{bmatrix}
$$
$$
\times
\begin{bmatrix}
\cos\left(\dfrac{k_{ph}d}{2}\right) & iZ_c \sin\left(\dfrac{k_{ph}d}{2}\right) \\
\dfrac{i}{Z_c} \sin\left(\dfrac{k_{ph}d}{2}\right) & \cos\left(\dfrac{k_{ph}d}{2}\right)
\end{bmatrix}, \tag{11}
$$

with k_{ph} and Z_c being the wavenumber and acoustic characteristic impedance in the waveguide respectively, which are given by:

$$k_{ph} = \frac{\omega_{ph}}{c_0} \left[1 + \frac{1-i}{\sqrt{\omega_{ph}\rho_0 r^2/\eta}} \left(1 + \frac{\gamma - 1}{\sqrt{Pr}} \right) \right], \tag{12}$$

$$Z_c = \frac{\rho_0 c_0}{\pi r^2} \left[1 + \frac{1-i}{\sqrt{\omega_{ph}\rho_0 r^2/\eta}} \left(1 + \frac{\gamma - 1}{\sqrt{Pr}} \right) \right]. \tag{13}$$

Here, γ is the specific heat ratio, Pr is the Prandtl number, η is the shear viscosity, while $Z_{H(n)}$ is the impedance of n-th side hole. Based on the experimental results, we conclude that the nonlinear losses, appearing at high level sound pressures due to jet and vortices formation at the locations of side holes, must be taken into account, i.e., here, $Z_{H(n)}$ is the sum of a linear impedance, Z_L, and a nonlinear one, $Z_{NL(n)}$, namely:

$$Z_{H(n)} = Z_L + Z_{NL(n)}. \tag{14}$$

On the one hand, the linear impedance of the hole can be expressed as a combination of the impedance of the hole plus the radiation impedance [48],

$$Z_L = iZ_{cH} \tan\left[k_H^{ph}(l_H + \Delta l_{Hi} + \Delta l_{Ho})\right] - \frac{1}{2}Z_{cH}\left(k_H^{ph}r_H\right)^2, \tag{15}$$

where Δl_{Hi} and Δl_{Ho} are length corrections due to the radiation inside the side holes and the radiation to the outer environment, while k_H^{ph} and Z_{cH} are the wavenumber and acoustic characteristic impedance in the side holes, obtained from Eq. (12) and Eq. (13) by using r_H instead of r. On the other hand, the nonlinear part of the impedance of n-th hole, $Z_{NL(n)}$, can be written as [42, 43],

$$Z_{NL(n)} = \beta_H Z_{cH} M_{(n)} St_{(n)}^{1/3}. \tag{16}$$

where β_H is a fitting parameter, which can be directly obtained by experiments. In addition, $M_{(n)}$ is the acoustic Mach number for n-th side hole, given by:

$$M_{(n)} = \frac{v_n}{c_0} = \frac{u_n/S_H}{c_0}, \tag{17}$$

with $u_n = v_n S_H$ being the volume velocity in the n-th side hole, while $St_{(n)}$ is the acoustic Strouhal number [42, 43, 49].

$$St_{(n)} = \frac{\omega_{ph}r_H}{v_n} = \frac{\omega_{ph}r_H}{u_n/S_H}. \tag{18}$$

Therefore, through $M_{(n)}$ and $St_{(n)}$, the nonlinear part $Z_{NL(n)}$ of the n-th side hole impedance depends explicitly on the local volume velocity u_n in n-th hole. However, the volume velocity is related to the impedance through

$$u_n = \frac{p_{(n)}}{Z_L + Z_{NL(n)}}. \tag{19}$$

Thus, we have to make some approximations, and apply an iterative method to calculate u_n. At the N-th hole, i.e., the last hole away from the source, the local volume velocity is the smallest compared to others, hence we can assume at first that the nonlinear part is zero at this position, $Z_{NL(n=N)} = 0$. From this hypothesis, we obtain the local volume velocity, $u_{(n=N)} = p_{(n=N)}/Z_L$ at this location. Here, it is noted that $p_{(n=N)}$ can be calculated by the following matrix,

$$
\begin{bmatrix} p_{(n=N)} \\ u_{\mathrm{w}(n=N)} \end{bmatrix} = \begin{bmatrix} \cos\left(k_{ph}D\right) & iZ_c \sin\left(k_{ph}D\right) \\ \dfrac{i}{Z_c} \sin\left(k_{ph}D\right) & \cos\left(k_{ph}D\right) \end{bmatrix} \begin{bmatrix} p^+ \\ p^+/Z_c \end{bmatrix}, \tag{20}
$$

where p^+ is positive-going wave at the end of waveguide (there is no negative-going wave due to the presence of the anechoic termination). Therefore,

$$
p^+ = \frac{i\left(p_{M-1}e^{-ik_{ph}x_M} - p_M e^{-ik_{ph}x_{M-1}}\right)}{2\sin\left[k_{ph}(x_{M-1} - x_M)\right]}e^{-ik_{ph}\frac{x_{M-1}+x_M}{2}}, \tag{21}
$$

where p_{M-1} and p_M are acoustic pressures measured at x_{M-1}, x_M by the microphone near the anechoic termination, p^+ is located at the center of p_{M-1} and p_M [i.e., at $(x_{M-1} + x_M)/2$], D is the distance between $p_{(n=N)}$ and p^+, and $u_{w(n=N)}$ is volume velocity in the waveguide.

This way, we obtain the local volume velocity, $u_{(n=N)}$, and substitute it into Eqs. (16)-(18). Then, the nonlinear impedance of the last hole, as well as the transfer matrix $T_{n=N}$ of last cell, can easily be derived. A similar iterative calculation can be applied considering that, in each iteration, first we approximate $Z_{NL(n)} = Z_{NL(n+1)}$. This procedure allows us to calculate the local volume velocity in the hole, and then the nonlinear impedance of the hole.

Up to now, we have the space-dependent nonlinear impedance of holes with different amplitudes of wave excitations. Then we can derive the transfer matrix of each cell, T_n, as well as the total transfer matrix, T, see Eqs. (10) and (11). Analytical reflection, transmission and absorption coefficients can be found by the total transfer matrix T.

4. Results and discussion

In this section, we start by discussing the experimental results. Firstly, we perform the experiment with a small-amplitude source. Here we choose 100 dB (linear limit), see black circles in **Figure 3**. Then, we change the amplitude of the source, for example, 120 dB (green squares), 130 dB (blue stars) and 140 dB (red triangles). The bigger the amplitude of the source is, the stronger the nonlinear effect, as well as nonlinear losses are. As a results, when the amplitude of the source is increased, maximum value of the absorption coefficient increases, and its bandwidth broadens. Here we have to highlight that in the low frequency, for example 200 Hz, the absorption coefficient in the case of 140 dB is 8 times larger than that in the case of 100 dB. These preliminary results pave the way to design the nonlinear acoustic absorber.

These experimental phenomenon could be analytically explained by the transfer matrix method, as shown in Section 3, using a nonlinear impedance model for the side-holes (see solid lines in **Figure 3**). Here we have to mention that β_H is a fitting parameter [Eq. (16)], because the nonlinear impedance of hole also depends on the amplitude of the wave excitation: the larger the amplitude, the larger the nonlinear impedance of holes, i.e., the larger β_H. In the linear limit (small source amplitude), there are no nonlinear losses for holes, i.e., $\beta_H = 0$. We use these rules to find the value of this fitting parameter, β_H, by comparing directly with the experimental results. In Refs. [50, 51], β_H is determined by means of numerical simulations: Disselhorst and Wijngaarden [50] found values of β_H between 0.6 and 1.0, while Peters and Hirschberg [51] evaluate β_H to 0.2. In our case, by direct comparison with
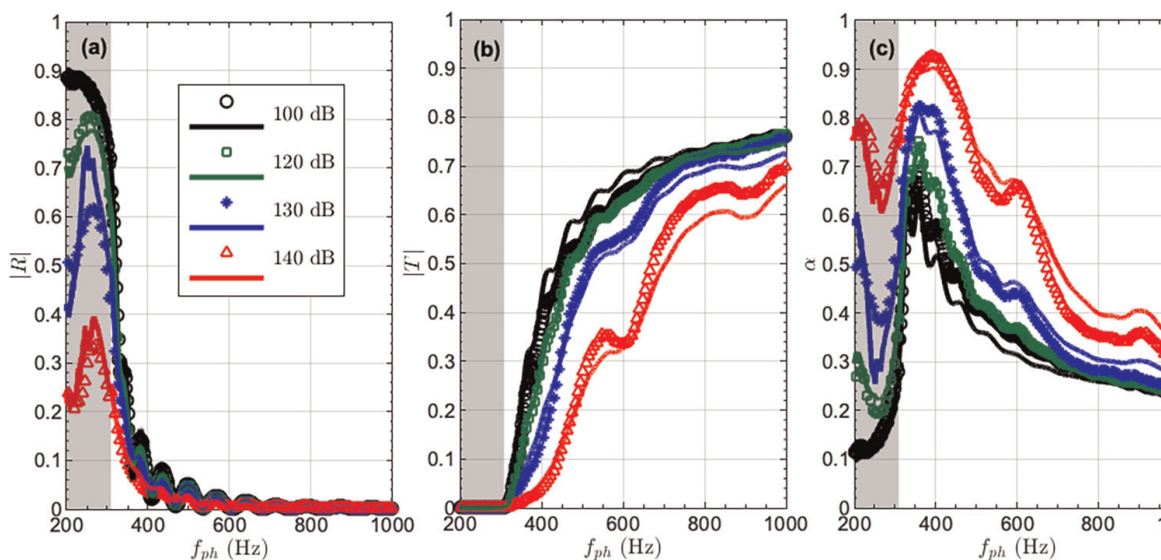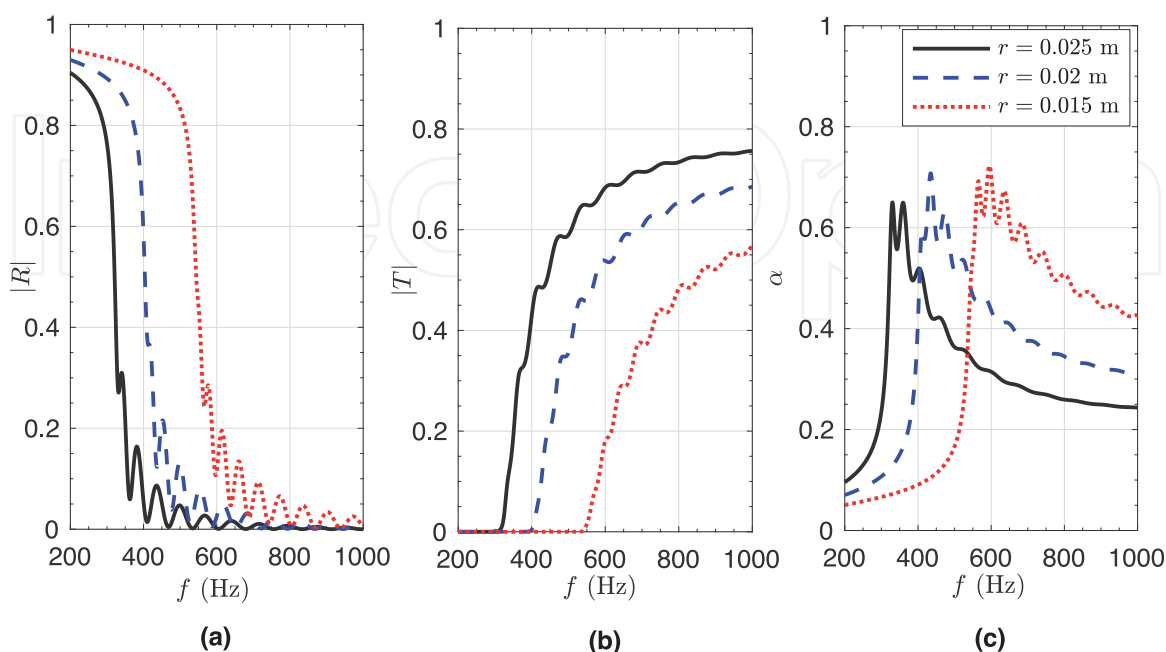
Figure 3.
(color online) amplitude of the (a) reflection coefficients, (b) transmission coefficients and (c) absorption coefficients adapted from ref. [44]. Black circles (lines), green squares (lines), blue stars (lines) and red triangles (lines) present the experimental (analytical) results with a source level around 100 dB, 120 dB, 130 dB, and 140 dB, respectively.

experiments, we found that β_H depends on the amplitude as $\beta_{H(140\ dB)} = 0.6$, $\beta_{H(130\ dB)} = 0.4$, $\beta_{H(120\ dB)} = 0.3$, while $\beta_{H(100\ dB)} = 0$ (linear case), i.e., the side holes feature no nonlinear losses when the amplitude of the source is small ($\lesssim 100$ dB). In the experiments, we have also observed the creation of flow through the holes, which led us to correct the length l_H by adding 0.0005 m. This value is independent of the amplitude. Comparing to other works [51–53], we have: $l_H = 0.005$ m, $\Delta l_{Hi} = 0.0027$ m and $\Delta l_{Ho} = 0.0026$ m, i.e., $l_H + \Delta l_{Hi} + \Delta l_{Ho} = 0.0103$ m; hence, the value of 0.0005 m is small, but cannot be ignored (**Figures 3** and **4**).
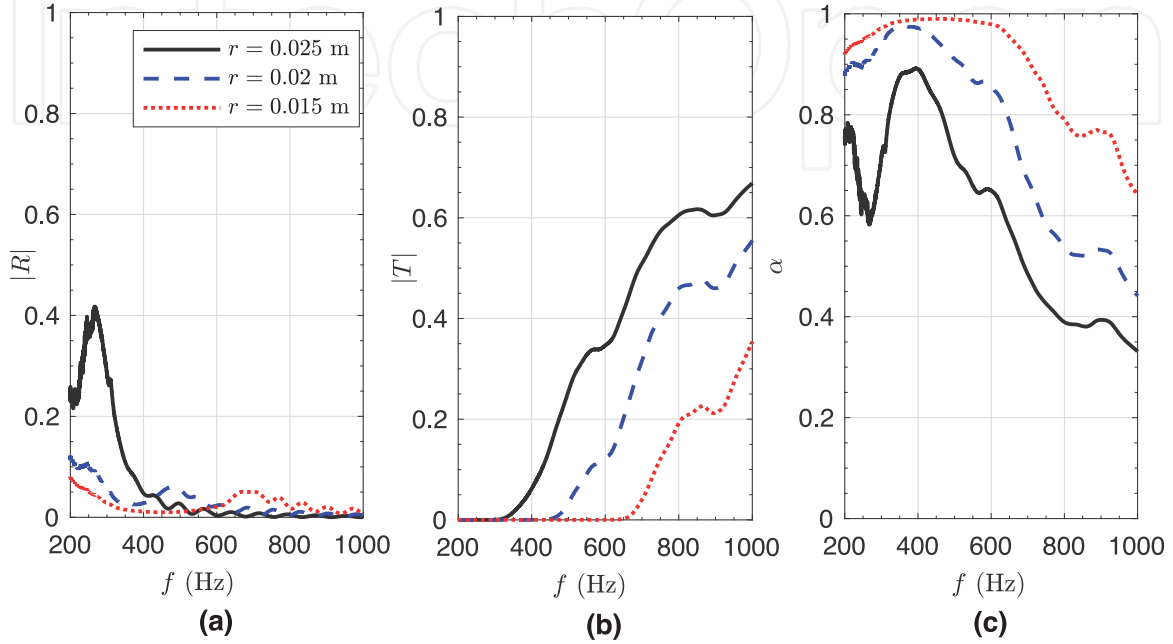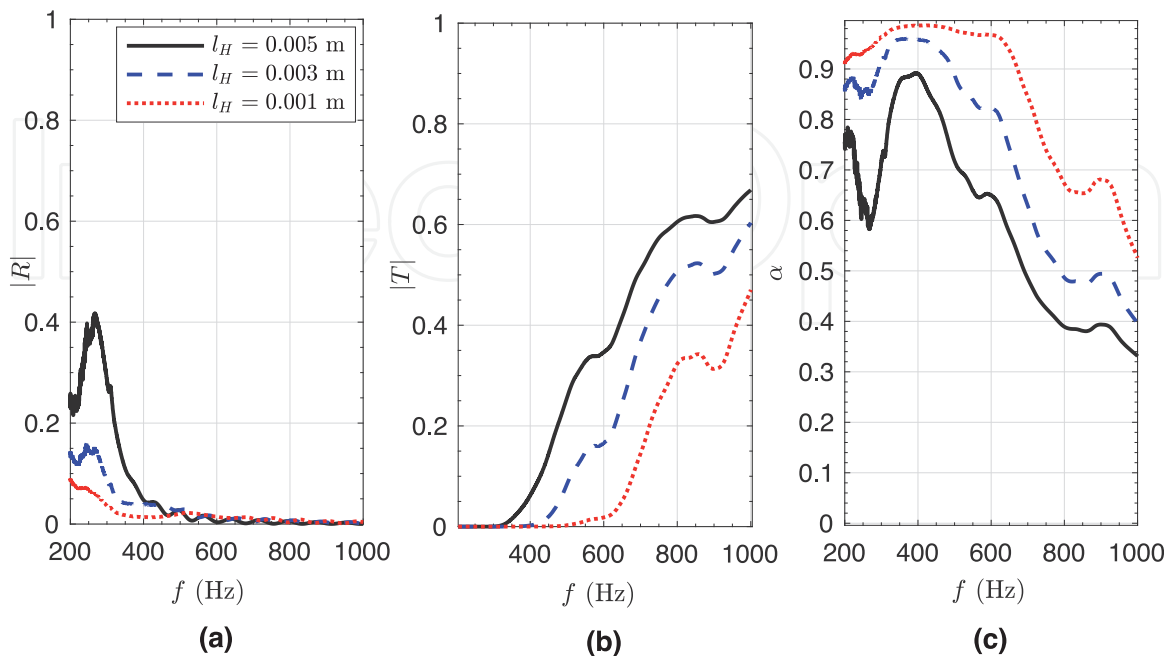

Figure 4.
(color online) amplitude of the (a) reflection coefficients, (b) transmission coefficients and (c) absorption coefficients. Black lines (r = 0.025 m), blue dashed lines (r = 0.02 m), red dotted lines (r = 0.015 m) present the analytical results with a source level around 100 dB (linear case).

Now we tune the parameters of the device in order to design an 1D amplitude-dependent acoustic perfect absorber. Here, we choose a source level around 140 dB. Firstly, when we decrease the radius of the waveguide, see **Figure 5**, the amplitude and the width of the absorption coefficient increase. Especially in the range of 400 – 600 Hz, the absorption coefficient is close to 1. We also found that decreasing the length of the side holes (see **Figure 6**) or increasing the radius of the side holes (see **Figure 7**) could improve the sound absorption of the meta-material. Finally, by

Figure 5.
(color online) amplitude of the (a) reflection coefficients, (b) transmission coefficients and (c) absorption coefficients. Black lines (r = 0.025 m), blue dashed lines (r = 0.02 m), red dotted lines (r = 0.015 m) present the analytical results with a source level around 140 dB (nonlinear case).

Figure 6.
(color online) amplitude of the (a) reflection coefficients, (b) transmission coefficients and (c) absorption coefficients. Black lines (l_H = 0.005 m), blue dashed lines (l_H = 0.003 m), red dotted lines (l_H = 0.001 m) present the analytical results with a source level around 140 dB (nonlinear case).
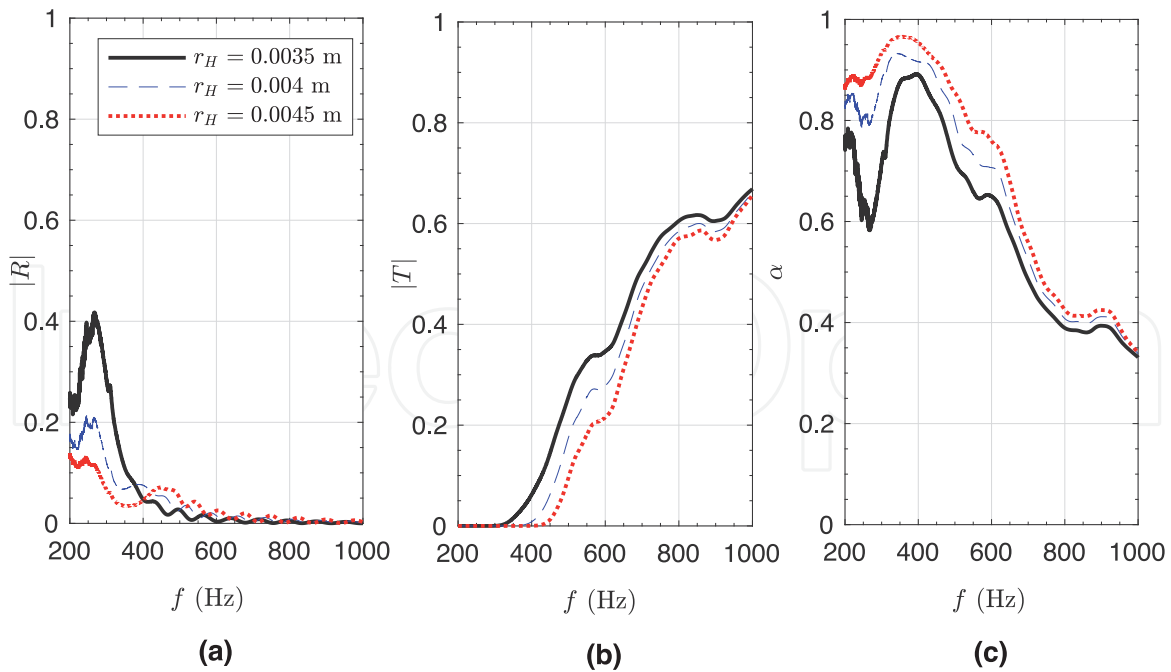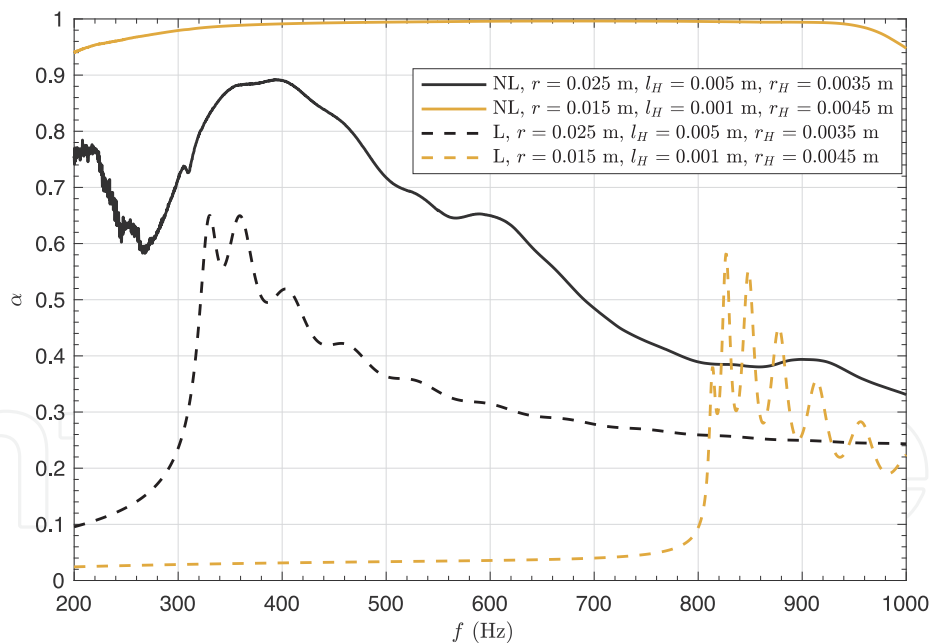
Figure 7.
(color online) amplitude of the (a) reflection coefficients, (b) transmission coefficients and (c) absorption coefficients. Black lines ($r_H = 0.0035\ m$), blue dashed lines ($r_H = 0.004\ m$), red dotted lines ($r_H = 0.0045\ m$) present the analytical results with a source level around 140 dB (nonlinear case).

Figure 8.
(color online) amplitude of the absorption coefficients. Black dashed lines ($r = 0.025\ m$, $l_H = 0.005\ m$, $r_H = 0.0035\ m$) and yellow dashed lines ($r = 0.015\ m$, $l_H = 0.001\ m$, $r_H = 0.0045\ m$) present the analytical results with a source level around 100 dB (linear case). Black solid lines ($r = 0.025\ m$, $l_H = 0.005\ m$, $r_H = 0.0035\ m$) and yellow solid lines ($r = 0.015\ m$, $l_H = 0.001\ m$, $r_H = 0.0045\ m$) present the analytical results with a source level around 140 dB (nonlinear case).

optimizing the parameters of the device, we choose $r = 0.015$ m, $l_H = 0.001$ m, $r_H = 0.0045$ m, see **Figure 8**. Now, in a wide frequency range, i.e., 300–900 Hz, the absorption coefficient equal to 1. Even in the range of 200–300 Hz or 900–1000 Hz, the absorption coefficient is not equal to one, however it is greater than 0.9.

5. Conclusions

In conclusion, we have analytically designed a large band amplitude-dependent acoustic absorber. We have studied nonlinear wave propagation in an 1D air-filled waveguide periodically side loaded by holes. We have performed the experiments to highlight the nonlinear losses effect. Transfer matrix theory could analytically capture the experimental phenomenon. Additionally, we analytically tune the parameter of the device and design a large band amplitude-dependent acoustic absorber. Our results concerning nonlinear losses, especially regarding the observed large value of the absorption coefficient in a relatively large bandwidth.

Acknowledgements

Author details

Jiangyi Zhang[1,2]

1 Harbin Engineering University, College of Underwater Acoustic Engineering, Harbin, China

2 le Mans Université, Laboratoire d'Acoustique de l'Université du Mans (LAUM), UMR CNRS 6613, Institut d'Acoustique-Graduate School (IA-GS), CNRS, Le Mans, France

*Address all correspondence to: zhangjiangyi0607@gmail.com

IntechOpen

References

[1] Lee D, Nguyen DM, Rho J. Acoustic wave science realized by metamaterials. Nano convergence. 2017;**4**:3

[2] Veselago VG. The electrodynamics of substances with simultaneously negative values of μ and ε. Soviet Physics Uspekhi. 1968;**10**(4):509-514

[3] Liu Z, Zhang X, Mao Y, Zhu YY, Yang Z, Chan CT, et al. Locally resonant sonic materials. Science. 2000;**289**:1734

[4] Liang B, Yuan B, Cheng JC. Acoustic diode: Rectification of acoustic energy flux in one-dimensional systems. Physical Review Letters. 2009;**103**: 104301

[5] Li X-F, Xu N, Liang F, Lu M-H, Cheng H, Chen Y-F. Tunable unidirectional sound propagation through a sonic-crystal based acoustic diode. Physical Review Letters. 2011; **106**:084301

[6] Li J, Fok L, Yin X, Bartal G, Zhang X. Experimental demonstration of an acoustic magnifying hyperlens. Nature Mater. 2009;**8**:931-934

[7] Climente A, Torrent D, Sanchez-Dehesa J. Sound focusing by gradient index sonic lenses. Applied Physics Letters. 2010;**97**:104103

[8] Welter JT, Sathish S, Christensen DE, Brodrick PG, Cherry MR. Focusing of longitudinal ultrasonic waves in air with an aperiodic flat lens. The Journal of the Acoustical Society of America. 2011;**130**: 27892796

[9] Zhao J, Bonello B, Boyko O. Focusing of the lowest-order antisymmetric lamb mode behind a gradient-index acoustic metalens with local resonators. Physical Review B. 2016;**93**:174306

[10] Xu N, He C, Sun X-C, Liu X p, Lu M-H, Feng L, et al. Topologically protected one-way edge mode in networks of acoustic resonators with circulating air flow. New Journal of Physics. 2015;**17**: 053016

[11] Peano V, Brendel C, Schmidt M, Marquardt F. Topological phases of sound and light. Physical Review X. 2015;**5**:031011

[12] Peng Y-G, Qin C-Z, Zhao D-G, Shen Y-X, Xu X-Y, Bao M, et al. Experimental demonstration of anomalous floquet topological insulator for sound. Nature Communications. 2016;**7**:13368

[13] Cummer SA, Schurig D. One path to acoustic cloaking. New Journal of Physics. 2007;**9**:45

[14] Chen H, Chan CT. Acoustic cloaking in three dimensions using acoustic metamaterials. Applied Physics Letters. 2007;**91**:183518

[15] Torrent D, Sanchez-Dehesa J. Acoustic cloaking in two dimensions: A feasible approach. New Journal of Physics. 2008;**10**:063015

[16] Shamonina E, Solymar L. Waves in Metamaterials. New york edition: Oxford University Press; 2009

[17] Henríquez VC, García-Chocano VM, Sánchez-Dehesa J. Viscothermal losses in double-negative acoustic metamaterials. Physical Review Applied. 2017;**8**:014029

[18] Gracía-Salgado R, García-Chocano V, Torrent D, Sánchez-Dehesa J. Negative mass density and density-near-zero quasi-two-dimensional metamaterial: Design and applications. Physical Review B. 2013;**88**:224305

[19] Guild MD, García-Chocano VM, Kan W, Sánchez-Dehesa J. Acoustic metamaterial absorbers based on multilayered sonic crystals. Journal of Applied Physics. 2015;**117**:114902

[20] Romero-Garcia V, Theocharis G, Richoux O, Merkel A, Tournat V, Pagneux V. Perfect and broadband acoustic absorption by critically coupled sub-wavelength resonators. Scientific Reports. 2016;**6**:19519

[21] Theocharis G, Romero-Garcá V, Richoux O, Tournat V. Limits of slow sound propagation and transparency in lossy, locally resonant periodic structures. New Journal of Physics. 2014; **16**:093017

[22] Ma G, Yang M, Xiao S, Yang Z, Sheng P. Acoustic metasurface with hybrid resonances. Nature Materials. 2014;**13**:873-878

[23] Lapine M, Shadrivov IV, Kivshar YS. Colloquium: Nonlinear metamaterials. Reviews of Modern Physics. 2014;**86**:1093

[24] Shalaev MI, Myslivets SA, Slabko VV, Popov AK. Negative group velocity and three-wave mixing in dielectric crystals. Optics Letters. 2011; **36**(19):38613

[25] Khurgin JB. Optical parametric oscillator: Mirrorless magic. Nature Photonics. 2007;**1**:446447

[26] Popov AK, Slabko VV, Shalaev VM. Second harmonic generation in left-handed metamaterials. Laser Physics Letters. 2006;**3**(6):293

[27] Hamilton M, Blackstock DT. Nonlinear Acoustics. San Diego, CA: Academic Press; 1998

[28] Sánchez-Morcillo VJ, Pérez-Arjona I, Romero-Garcá V, Tournat V, Gusev VE. Second-harmonic generation for dispersive elastic waves in a discrete granular chain. Physical Review E. 2013; **88**:043203

[29] Jiménez N, Mehrem A, Picó R, García-Ra LM, Sánchez-Morcillo VJ. Nonlinear propagation and control of acoustic waves in phononic superlattices. Comptes Rendus Physique. 2016;**17**: 543554

[30] Zhang J, Romero-García V, Theocharis G, Richoux O, Achilleos V, Frantzeskakis DJ. Second-harmonic generation in membrane-type nonlinear acoustic metamaterials. Crystals. 2016; **6**(8):86

[31] Boechler N, Theocharis G, Daraio C. Bifurcation-based acoustic switching and rectification. Nature Mater. 2011;**10**:665

[32] Devaux T, Tournat V, Richoux O, Pagneux V. Asymmetric acoustic propagation of wave packets via the self-demodulation effect. Physical Review Letters. 2015;**115**:234301

[33] Khajehtourian R, Hussein MI. Dispersion characteristics of a nonlinear elastic metamaterial. AIP Advances. 2014;**04**:124308

[34] Donahue CM, Anzel PWJ, Bonanomi L, Keller TA, Daraio C. Experimental realization of a nonlinear acoustic lens with a tunable focus. Applied Physics Letters. 2014;**104**: 014103

[35] Manktelow K, Leamy MJ, Ruzzene M. Multiple scales analysis of wavewave interactions in a cubically nonlinear monoatomic chain. Nonlinear Dynamics. 2011;**63**:193

[36] Boechler N, Job S, Kevrekidis PG, Theocharis G, Porter MA, Daraio C. Discrete breathers in one-dimensional

diatomic granular crystals. Physical Review Letters. 2010;**104**:244302

[37] Averkiou MA, Lee YS, Hamilton MF. Self-demodulation of amplitude and frequency modulated pulses in a thermoviscous fluid. The Journal of the Acoustical Society of America. 1993;**94**(5):28762883

[38] Vos HJ, Goertz DE, de Jong N. Self-demodulation of high-frequency ultrasound. The Journal of the Acoustical Society of America. 2010;**127**(3):1208-1217

[39] Sugimoto N, Masuda M, Ohno J, Motoi D. Experimental demonstration of generation and propagation of acoustic solitary waves in an air-filled tube. Physical Review Letters. 1999;**83**:4053

[40] Achilleos V, Richoux O, Theocharis G, Frantzeskakis DJ. Acoustic solitons in waveguides with helmholtz resonators: Transmission line approach. Physical Review E. 2015;**91**:023204

[41] Zhang J, Romero-García V, Theocharis G, Richoux O, Achilleos V, Frantzeskakis DJ. Bright and gap solitons in membrane-type acoustic metamaterials. Physical Review E. 2017;**96**:022214

[42] Atig M, Dalmont J, Gilbert J. Termination impedance of open-ended cylindrical tubes at high sound pressure level. Comptes Rendus Mécanique. 2004;**332**(4):299-304

[43] Buick JM, Skulina AMD, Campbell D, Dalmont JP, Gilbert J. Investigation of non-linear acoustic losses at the open end of a tube. The Journal of the Acoustical Society of America. 2011;**129**(3):1261-1272

[44] Zhang J, Romero-García V, Theocharis G, Richoux O, Achilleos V, Frantzeskakis DJ. High-amplitude sound propagation in acoustic transmission-line metamaterial. Applied Physics Letters (Editors' Pick). 2021;**118**:104102

[45] Dalmont JP. Study and Realization of Acoustic Impedance Sensors. Application to Measurements of Lumped Elements. Study and Realization of an Anechoic Termination for Low Frequencies, Ph.D. thesis. University of Maine, HAL; 1988

[46] Song BH, Bolton JS. A transfer-matrix approach for estimating the characteristic impedance and wave numbers of limp and rigid porous materials. The Journal of the Acoustical Society of America. 2000;**107**:1131

[47] Pierce AD. Acoustics: An Introduction to its Physical Principles and Applications. New York: McGraw-Hill; 1981

[48] Zwikker C, Kosten CW. Sound Absorbing Materials. New York: Elsevier; 1949

[49] Temiz MA, Tournadre J, Arteaga IL, Hirschberg A. Non-linear acoustic transfer impedance of micro-perforated plates with circular orifices. Journal of Sound and Vibration. 2016;**366**:418-428

[50] Disselhorst J, Wijngaarden LV. Flow in the exit of open pipes during acoustic resonance. Journal of Fluid Mechanics. 1980;**99**(2):293-319

[51] Peters M, Hirschberg A. Acoustically induced periodic vortex shedding at sharp edged open channel ends: Simple vortex models. Journal of Sound and Vibration. 1993;**161**(2):281-299

[52] Kalozoumis PA, Richoux O, Diakonos FK, Theocharis G. Invariant

currents in lossy acoustic waveguides with complete local symmetry. Physical Review B. 2015;**92**:014303

[53] Dubos V, Kergomard J, Keefe D, Dalmont J-P, Khettabi A, Nederveen K. Theory of sound propagation in a duct with a branched tube using modal decomposition. Acta Acustica united with Acustica. 1999;**85**(2):153-169

[54] Dalmont J-P, Nederveen CJ, Joly N. Radiation impedance of tubes with different flanges: Numerical and experimental investigations. Journal of Sound and Vibration. 2001;**244**(3): 505-534